Article

On the Functional Role of a Water Molecule in Clade 3 Catalases: A Proposal for the Mechanism by Which NADPH Prevents the Formation of Compound II

Willi Sicking, Hans-Gert Korth, Herbert de Groot, and Reiner Sustmann

J. Am. Chem. Soc., **2008**, 130 (23), 7345-7356 • DOI: 10.1021/ja077787e • Publication Date (Web): 15 May 2008

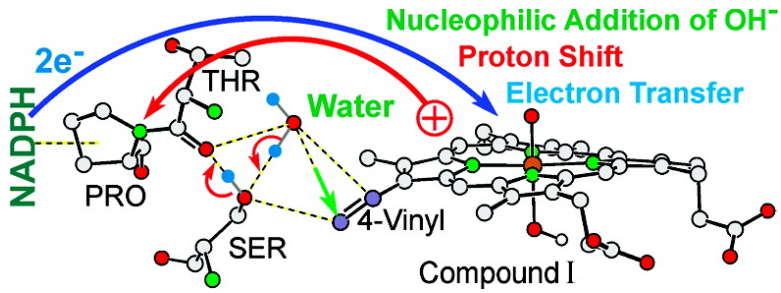

More About This Article

Additional resources and features associated with this article are available within the HTML version:

- Supporting Information
- Links to the 3 articles that cite this article, as of the time of this article download
- Access to high resolution figures
- Links to articles and content related to this article
- Copyright permission to reproduce figures and/or text from this article

View the Full Text HTML

J|A|C|S
ARTICLES

Published on Web 05/15/2008

On the Functional Role of a Water Molecule in Clade 3 Catalases: A Proposal for the Mechanism by Which NADPH Prevents the Formation of Compound II

Willi Sicking,[†] Hans-Gert Korth,[†] Herbert de Groot,[‡] and Reiner Sustmann*,[†]

Institut für Organische Chemie, Universität Duisburg-Essen, 45117 Essen, Germany, and Institut für Physiologische Chemie, Universitätsklinikum Essen, 45122 Essen, Germany

Received October 10, 2007; E-mail: reiner.sustmann@uni-duisburg-essen.de

Abstract: X-ray structures of the 13 different monofunctional heme catalases published to date were scrutinized in order to gain insight in the mechanism by which NADPH in Clade 3 catalases may protect the reactive ferryloxo intermediate Compound I (Cpd I; por$^{\bullet+}$Fe^{IV}=O) against deactivation to the catalytically inactive intermediate Compound II (Cpd II; porFe^{IV}=O). Striking similarities in the molecular network of the protein subunits encompassing the heme center and the surface-bound NADPH were found for all of the Clade 3 catalases. Unique features in this region are the presence of a water molecule (W1) adjacent to the 4-vinyl group of heme and a serine residue or a second water molecule hydrogen-bonded to both W1 and the carbonyl group of a threonine−proline linkage, with the proline in van der Waals contact with the dihydronicotinamide group of NADPH. A mechanism is proposed in which a hydroxyl anion released from W1 undergoes reversible nucleophilic addition to the terminal carbon of the 4-vinyl group of Cpd I, thereby producing a neutral porphyrin π-radical ferryloxo (HO−por$^{\bullet}$Fe^{IV}=O) species of reduced reactivity. This structure is suggested to be the elusive Cpd II′ intermediate proposed in previous studies. An accompanying proton-shifting process along the hydrogen-bonded network is believed to facilitate the NADPH-mediated reduction of Cpd I to ferricatalase and to serve as a funnel for electron transfer from NADPH to the heme center to restore the catalase Fe^{III} resting state. The proposed reaction paths were fully supported as chemically reasonable and energetically feasible by means of density functional theory calculations at the (U)B3LYP/6-31G* level. A particularly attractive feature of the present mechanism is that the previously discussed formation of protein-derived radicals is avoided.

Introduction

Heme catalases belong to the longest-known and best-studied families of enzymes. Their function is regulation of the hydrogen peroxide level in living cells by conversion of H_2O_2 to water and oxygen (eq 1). The diversity of structures and properties of catalases has been summarized in a number of reviews.[1–9]

$$2H_2O_2 \rightarrow 2H_2O + O_2 \quad (1)$$

Catalases are generally divided into three classes. The most abundant class (Class 1) encompasses monofunctional catalases, while the second includes bifunctional catalase-peroxidases and the third nonheme, manganese-containing enzymes. All heme catalases are composed of four identical subunits, each of which contains an active heme site. Presently, there are more than 225 Class 1 catalases known.[3] Only catalases in this class are subjects of the present study. Class 1 catalases are subdivided based on large (>75 kDa) or small (<60 kDa) subunits. According to phylogenetic analyses, three subgroups, or *clades*, can be distinguished.[2,3,10] Clade 2 contains catalases with large subunits and heme *d*, while those in Clades 1 and 3 have small subunits and heme *b*. Clade 3 catalases are characterized by a tightly surface-bound NADPH molecule in each subunit and are among the evolutionally youngest catalases. The role of the two-electron reductant NADPH in Clade 3 catalases has been studied, and different proposals for its reducing activity have been made.[11–17]

The mechanism by which the disproportionation of H_2O_2 (eq 1) takes place has been extensively studied and is in general

[†] Universität Duisburg-Essen.
[‡] Universitätsklinikum Essen.

(1) Zamocky, M.; Koller, F. *Prog. Biophys. Mol. Biol.* **1999**, *72*, 19–66.
(2) Nicholls, P.; Fita, I.; Loewen, P. C. *Adv. Inorg. Chem.* **2001**, *51*, 51–106.
(3) Chelikani, P.; Fita, I.; Loewen, P. C. *Cell. Mol. Life Sci.* **2004**, *61*, 192–208.
(4) Kirkman, H. N.; Gaetani, G. F. *Trends Biochem. Sci.* **2007**, *32*, 44–50.
(5) Bartosz, G. *Handb. Environ. Chem.* **2005**, *2*, 109–149.
(6) Putnam, C. D.; Arvai, A. S.; Bourne, Y.; Tainer, J. A. *J. Mol. Biol.* **2000**, *296*, 295–309.
(7) Schonbaum, G. R.; Chance, B. In *The Enzymes*, 3rd ed.; Boyer, P. D., Ed.; Academic Press: New York, 1976; Vol. 13, pp 363−408.
(8) Deisseroth, A.; Dounce, A. L. *Physiol. Rev.* **1970**, *50*, 319–375.
(9) Nicholls, P.; Schonbaum, G. R. In *The Enzymes*, 2nd ed.; Boyer, P. D., Lardy, H., Myrbäck, K., Eds.; Academic Press: New York, 1963; Vol. 8, pp 147−225.
(10) Klotz, M. G.; Loewen, P. C. *Mol. Biol. Evol.* **2003**, *20*, 1098–1112.
(11) Kirkman, H. N.; Galiano, S.; Gaetani, G. F. *J. Biol. Chem.* **1987**, *262*, 660–666.
(12) Almarsson, Ö.; Sinha, A.; Gopinath, E.; Bruice, T. C. *J. Am. Chem. Soc.* **1993**, *115*, 7093–7102.
(13) Hillar, A.; Nicholls, P.; Switala, J.; Loewen, P. C. *Biochem. J.* **1994**, *300*, 531–539.
(14) Olson, L. P.; Bruice, T. C. *Biochemistry* **1995**, *34*, 7335–7347.

Scheme 1. Catalytic Cycle of Hydrogen Peroxide Decomposition by Clade 3 Heme Catalases

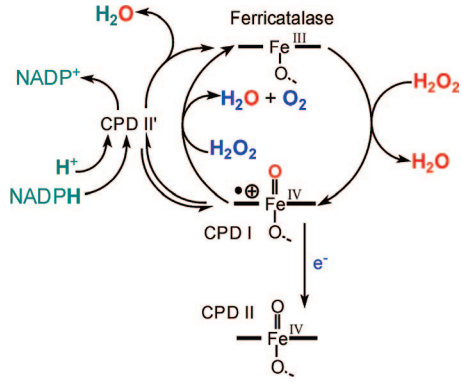

well-understood (Scheme 1). According to this mechanism, the first step of H_2O_2 decomposition involves reaction of the enzyme's Fe^{III} resting state (ferricatalase) with one molecule of H_2O_2 to generate a highly reactive ferryloxoporphyrin radical cation species ($por^{\bullet+}Fe^{IV}$=O) called Compound I (Cpd I)[7,9,18–22] and a water molecule. In the next step, a second molecule of H_2O_2 acts as a reductant for Cpd I, leading to release of molecular oxygen and water and conversion of the enzyme back to the resting state. However, because of the strong oxidizing power of Cpd I, competitive side reactions that eventually may terminate the catalatic cycle can occur. Preferably, the surrounding protein may deliver an electron to Cpd I, converting it to Compound I* (Cpd I*; $porFe^{IV}$=O/protein$^{\bullet}$), in which the porphyrin radical cation is re-reduced. One-electron quenching of the protein radical then produces Compound II (Cpd II; $porFe^{IV}$=O). Similarly, external one-electron donors may produce Cpd II directly. Cpd II, which may exist in two different protonation states,[2,22–24] is an inactive state with regard to H_2O_2 disproportionation. Although the mechanism of Scheme 1 is generally accepted, a number of facets that still await clarification remain. One of these issues is the mechanism by which Cpd I is protected from being deactived by one-electron reduction to Cpd II.[2] Accordingly, in a recent review that focused on the role of NADPH, Kirkman and Gaetani[4] called mammalian catalase "a venerable enzyme with new mysteries".

Formation of Cpd II is favored in situations where H_2O_2 production is low, i.e., where the second step of the catalatic cycle is kinetically disfavored as a result of a diminished supply of H_2O_2.[4,6] Accordingly, in a recent publication we provided evidence that at low hydrogen peroxide levels, catalase catalytically decomposes H_2O_2 without release of oxygen.[25] Formation of Cpd II from Clade 3 catalases has been detected only in the absence of NADPH, and therefore, it has been proposed that NADPH protects Cpd I against reduction by reductants other than H_2O_2.[2,4,6] It should be noted, however, that Cpd II is not effectively reduced to ferricatalase by the bound NADPH. This observation prompted Kirkman and co-workers[4,16] to postulate the occurrence of a not-yet-characterized Cpd I-derived intermediate called Compound II′ (Cpd II′) that uses NADPH to regenerate ferricatalase, thereby avoiding termination of the catalatic cycle.

In the present work, we scrutinized the 13 currently-available X-ray structures of heme catalases, with the goal of finding structural similarities or dissimilarities that may be related to the functional role of NADPH in Clade 3 catalases. As outlined below, analysis of the pertinent local structures of the various catalases revealed striking similarities among the Clade 3 NADPH-binding catalases, which differ grossly from the non-NADPH-binding Clade 1 and Clade 2 catalases. This analysis has led us to propose a chemically reasonable mechanism by which formation of Cpd II is avoided and electron transfer from the surface-bound NADPH to the heme center would be facilitated. The proposed mechanism is elucidated using density functional theory (DFT) calculations at the (U)B3LYP/6-31G* level. The quantum-chemical data are in general correspondence with the proposed mechanism and demonstrate that its reaction paths are chemically and energetically feasible.

Methods

Analysis of X-Ray Structures. All of the available X-ray data for monofunctional catalases were downloaded from the RCSB Protein Data Bank (PDB).[26] For catalases having multiple entries in the PDB, the most recent structures, which are generally also the ones of highest resolution, were selected for the final analysis (Table 1). From the computerized representation of the PDB data, the coordinates of the heme iron of subunit A were determined, and a sphere around the iron center with a radius of ~20 Å enclosing the NADPH binding site was cut out by means of the PERGRA program.[27] From the surface of this sphere, residues were then successively erased until the desired relevant structural features were worked out. Hydrogen atoms were added to the heavy atoms using standard bond lengths and angles by means of the Titan program,[28] which was also used for extraction of geometrical parameters. Graphics were prepared using PERGRA and refined using CorelDraw.[29]

Computational Procedures. DFT calculations at the (U)B3LYP/6-31G(d) level were performed using the Gaussian 03 suite of programs.[30] The basis of the calculations was the X-ray structure of human erythrocyte catalase (HEC) (PDB code 1DGF).[6] The heme center, the threonine (THR)−proline (PRO) couple adjacent to the surface-bound NADPH, and the water molecule and serine (SER) residue positioned between the 4-vinyl group of the heme and the THR−PRO linkage were cut out of the HEC X-ray structure. Because of the enormous computational effort, the structures had to be simplified, but the geometric integrity of the relevant motifs was preserved as far as possible. Details of the geometric restrictions are given in Tables S6 and S7 and associated text in the Supporting Information. Except for these restrictions, the molecular complexes were fully optimized with the inclusion of a polarizable continuum

(15) Bicout, D. J.; Field, M. J.; Gouet, P.; Jouve, H. M. *Biochim. Biophys. Acta* **1995**, *1252*, 172–176.
(16) Kirkman, H. N.; Rolfo, M.; Ferraris, A. M.; Gaetani, G. F. *J. Biol. Chem.* **1999**, *274*, 13908–13914.
(17) Ivancich, A.; Jouve, H. M.; Sartor, B.; Gaillard, J. *Biochemistry* **1997**, *36*, 9356–9364.
(18) Chance, B. *Acta Chem. Scand.* **1947**, *1*, 236–267.
(19) Chance, B. *Nature* **1948**, *161*, 914–917.
(20) Jouve, H. M.; Andreoletti, P.; Gouet, P.; Hajdu, J.; Gagnon, J. *Biochimie* **1997**, *79*, 667–671.
(21) Behan, R. K.; Green, M. T. *J. Inorg. Biochem.* **2006**, *100*, 448–459.
(22) Alfonso-Prieto, M.; Borovik, A.; Carpena, X.; Murshudov, G.; Melik-Adamyan, W.; Fita, I.; Rovira, C.; Loewen, P. C. *J. Am. Chem. Soc.* **2007**, *129*, 4193–4205.
(23) Rovira, C. *ChemPhysChem* **2005**, *6*, 1820–1826.
(24) Horner, O.; Mouesca, J. M.; Solari, P. L.; Orio, M.; Oddou, J. L.; Bonville, P.; Jouve, H. M. *J. Biol. Inorg. Chem.* **2007**, *12*, 509–525.
(25) De Groot, H.; Auferkamp, O.; Bramey, T.; De Groot, K.; Kirsch, M.; Korth, H.-G.; Petrat, F.; Sustmann, R. *Free Radical Res.* **2006**, *40*, 67–74.
(26) Research Collaboratory for Structural Bioinformatics. RCSB Protein Data Bank. http://www.rcsb.org/pdb/ (accessed May 5, 2008).
(27) Sustmann, R.; Sicking, W. PERGRA, version 2007; Universität Duisburg-Essen: Essen, Germany, 2007.
(28) Titan, version 1.0; Schrödinger, LLC: Portland, OR, 1999.
(29) CorelDRAW, version X3; Corel Corporation: Ottawa, ON, 2005.
(30) Frisch, M. J.; et al. Gaussian 03, revision C.02; Gaussian, Inc.: Wallingford, CT, 2004.

Table 1. Catalase X-Ray Structures Obtained From the PDB and Notation for Key Water Molecules and Amino Acid Residues in Proximity to the 1-Methyl and 4-Vinyl Groups of Heme

catalase description						
acronym	source	PDB code	resolution (Å)	water[a]	amino acid[a]	reference
		Clade 1				
CatF	*Pseudomonas syringae*	1M7S	1.80	HOH1786	VAL219	43
EKTA	*Exiguobacterium oxidotolerans*	2J2M	2.40	HOH60	VAL198	44
		Clade 2				
HPII	*Escherichia coli*	1GGE	1.89	HOH213	ILE274	45
PVC	*Penicillium vitale*	2IUF	1.71	HOH212	VAL210	22
NCC	*Neurospora crassa*	1SY7	1.75	HOH1223	VAL238	46
		Clade 3				
HEC	human erythrocyte[b]	1DGF	1.50	HOH223	SER217	6
BLC	bovine liver	4BLC	2.30	(see text)	SER216	47
MLC	*Micrococcus lysodeikticus*	1GWF[c]	1.96	HOH165	SER202	48
PMC	*Proteus mirabilis*[b]	1M85	2.00	HOH14	SER196	49
CatA	*Saccharomyces cerevisiae*	1A4E[d]	2.40	HOH671	HOH19	50
HPC	*Helicobacter pylori*	1QWL[e]	1.60	HOH420	SER198	51
EFC	*Enterococcus faecalis*	1SI8	2.30	HOH632	SER196	52
VSC	*Vibrio salmonicida*	2ISA	1.97	HOH758	SER196	53

[a] Adjacent to the 1-methyl group in Clade 1 and 2 catalases and to the 4-vinyl group in Clade 3 catalases. [b] Structures with and without bound NADPH are available (see Figure S3 in the Supporting Information). [c] Cpd II. [d] Azide bound to iron. [e] O_2 or HOO adduct (probably Cpd III).

environment (see below). The structures were analyzed for possible hydrogen-bonding motifs by placing a hydrogen atom on the line connecting the acceptor and donor atoms in the starting arrangement for the geometry optimization. The position of the second hydrogen atom of the water molecules then was established utilizing standard bond lengths and angles. Optimizations were carried out for various initial rotational orientations of the water molecules in order to locate the lowest-energy structure.

In a previous calculation of catalase Cpd I, Green[31] observed that using phenolate as the model for the proximal tyrosine (TYR) ligand of iron resulted in almost-complete transfer of an electron from the phenolate ligand to the porphyrin system, i.e., an almost-full unpaired spin was found on the phenolate ligand. However, when an arginine (ARG) molecule was hydrogen-bonded to the axial phenolate (as in the native enzyme), the unpaired spin remained mainly on the porphyrin moiety, as experimentally observed.[32] Following his procedure, we attached methylguanidinium to the proximal phenolate, thereby obtaining electron distributions similar to those reported previously.[31,33]

The protein environment was modeled using the conductor-like polarizable conductor (CPCM) model in the self-consistent reaction field (SCRF) method[34,35] with a dielectric constant of $\varepsilon = 5.7$[36] and a cavity defined using the UAO model. However, since average dielectric constants for a protein environment have been reported to range from 5.7 to 10.65,[37] we supplemented our study using single-point calculations with $\varepsilon = 10.65$ on the structures optimized with $\varepsilon = 5.7$. Absolute and relative energies are given in Tables S2 and S8 in the Supporting Information. Since the definition of an arbitrary dielectric constant does not correspond to the internal definition of other solvent-related parameters,[38] the structures were recalculated using the Gaussian SOLVENT keyword for solvents with similar dielectric constants, namely, chlorobenzene ($\varepsilon = 5.62$) and dichloroethane ($\varepsilon = 10.36$). The energies thus obtained differed by less than 0.4 kcal mol^{-1} from the values for $\varepsilon = 5.7$ and 10.65 (Table S3 in the Supporting Information). Transition structures (TSs) were determined using appropriate reaction-coordinate calculations (see p S12 in the Supporting Information). Since the sizes of the hydrogen-bonded networks prohibited frequency calculations on the full system, their zero-point vibrational energies (ZPVEs) were approximated as the sum of the ZPVEs of the individual components. Still, a simplified model for the heme moiety in which the proximal phenolate and methylguanidinium ligands were replaced by a hydroxyl anion had to be used. We observed that such a replacement preserved the spin distribution of the porphyrin−Fe═O system (Figure S12 in the Supporting Information). If the errors in ZPVE introduced by this procedure were similar for interconverting structures, our estimates of the ZPVE corrections (ΔZPVE) to the reaction energies would have been reasonably good.

Since the sizes of the systems required extensive computation time, geometry optimizations were carried out only to a convergence limit in which no change in the fourth decimal place of the total energy was found (i.e., $E_{i+1} - E_i \leq 0.0001$ au) for at least 10 consecutive cycles. Electronic properties such as dipole moments, NPA charges, and spin densities were then obtained from single-point calculations on these structures. The calculations were focused on the high-spin states of the iron complexes because it had previously been found that for reactive heme and nonheme ferryloxo species, the energies of the high-spin states are virtually identical to those of the low-spin states.[39–41] This was confirmed by the corresponding data for structures **A**, **B1**, and **4** (Table 2 and Tables S4 and S8 in the Supporting Information). The reliability of the present computational approach was supported by exploratory calculations on the two key species **A** and **B1** using the Los Alamos lanl2dz, Stuttgart-Dresden sdd, and B3LYP/6-311G[31] basis sets (Tables S4 and S5 in the Supporting Information). The relative energies obtained using these basis sets differed by less than 1.2 kcal mol^{-1} from the B3LYP/6-31G(d) data.

Results and Discussion

Catalase Structures. X-ray structures of 13 different catalases have been reported to date:[42] two Clade 1 catalases,[43,44] three

(31) Green, M. T. *J. Am. Chem. Soc.* **2001**, *123*, 9218–9219.
(32) Benecky, M. J.; Frew, J. E.; Scowen, N.; Jones, P.; Hoffman, B. M. *Biochemistry* **1993**, *32*, 11929–11933.
(33) Rydberg, P.; Sigfridson, E.; Ryde, U. *J. Biol. Inorg. Chem.* **2004**, *9*, 203–223.
(34) Cossi, M.; Rega, N.; Scalmani, G.; Barone, V. *J. Comput. Chem.* **2003**, *24*, 669–681.
(35) Barone, V.; Cossi, M. *J. Phys. Chem. A* **1998**, *102*, 1995–2001.
(36) de Visser, S. P.; Shaik, S.; Sharma, P. K.; Kumar, D.; Thiel, W. *J. Am. Chem. Soc.* **2003**, *125*, 15779–15788.
(37) de Visser, S. P. *J. Phys. Chem. A* **2005**, *109*, 11050–11057.
(38) Frisch, A. E.; Frisch, M. J.; Trucks, G. W. *Gaussian 03 User's Reference*; Gaussian, Inc.: Wallingford, CT, 2003; p 205.
(39) Shaik, S.; Hirao, H.; Kumar, D. *Acc. Chem. Res.* **2007**, *40*, 532–542.
(40) Shaik, S.; Kumar, D.; de Visser, S. P.; Altun, A.; Thiel, W. *Chem. Rev.* **2005**, *105*, 2279–2328.
(41) Sicking, W.; Korth, H.-G.; Jansen, G.; de Groot, H.; Sustmann, R. *Chem.—Eur. J.* **2007**, *13*, 4230–4245.

Table 2. Relative Energies (kcal mol^{-1}) at 0 K and Dipole Moments (D) for Different Values of the Dielectric Constant ε[a]

		$\varepsilon = 5.7$[b]		$\varepsilon = 10.65$[c]	
structure	model	E_{rel}[d]	μ	E_{rel}[d]	μ
A[e]	Cpd I	0.0	15.7	0.0	16.2
A[e] ($S = {}^1/_2$)	Cpd I	−0.1	15.8	−0.2	16.3
A[f]	Cpd I	+0.2	16.8	+0.2	17.3
A[g]	Cpd I	+1.0	16.3	+1.1	16.8
A[h]	Cpd I	+0.6	15.9	+0.7	16.4
B1	Cpd II′	−4.4	46.0	−5.3	46.9
B1 ($S = {}^1/_2$)	Cpd II′	−4.3	46.2	−5.3	47.1
B2	Cpd II′	−0.3	48.7	−1.6	49.6
1	Cpd I + imidazolium + NADPH[i]	0.0	15.4	0.0	15.8
2	Cpd II′ + imidazolium + NADPH	−0.3	41.4	−1.4	42.4
3	TS[RC] + imidazolium + NADPH	8.2	27.0	7.8	28.2
4	ferricatalase + imidazole + NADP$^+$[j]	−57.5	9.2	−56.5	9.4
5	Fe^{III}OH + imidazolium + NADP$^+$	−45.4	19.8	−47.8	20.4
6	Cpd II′(H$^+$) + imidazole + NADPH	−0.5	32.7	−1.6	33.6
7	Cpd I(H$^+$) + imidazole + NADPH	+12.9	14.2	+11.3	14.2
8	TS[RC](H$^+$) + imidazole + NADPH	+13.7[k]	13.6	12.6[l]	14.4
9	Cpd II + imidazolium	0.0	18.4	0.0	18.9
10	Cpd II(H$^+$) + imidazole (Fe^{IV})	−8.7	14.2	−5.4	14.3
11	Cpd II′(H$^+$) + e$^-$ + imidazole	−0.4	43.3	+1.5	44.4

[a] Obtained using the SCRF model at the B3LYP/6-31G(d) level; species were in the high-spin ($S = {}^3/_2$) state unless noted otherwise. [b] Dielectric constant used in the SCRF geometry optimization. [c] Dielectric constant used in single-point SCRF calculations on the $\varepsilon = 5.7$ geometry. [d] E_{rel} values are calculated with respect to the following energies: (**A**−**B2**) the energy of high-spin A with the position of O9 unconstrained and H pointing away from viewer; (**1**−**8**) the energy of **1**; (**9**−**11**) the energy of **9**. [e] Position of O9 unconstrained, H pointing away from viewer. [f] Position of O9 unconstrained, H pointing toward viewer. [g] Position of O9 locked and dihedral angle H10 constrained as in HEC. [h] Position of O9 locked as in HEC, H pointing away from viewer. [i] Modeled by 1-methyl-1,4-dihydropyridine-3-carboxylic acid amide (*N*-methyldihydronicotinamide, NMNAH). [j] Modeled by 1-methylpyridinium-3-carboxylic acid amide (NMNA$^+$). [k] [$E_{rel}(\varepsilon = 5.7)$ for **7**] + 0.8 kcal mol^{-1}. [l] [$E_{rel}(\varepsilon = 10.65)$ for **7**] + 1.3 kcal mol^{-1}.

Clade 2 catalases,[22,45,46] and eight Clade 3 catalases[6,47–53] (Table 1; details of amino acid sequences are given in Table S1 in the Supporting Information). As noted above, only Clade 3 catalases bind NADPH. In one of the Clade 3 catalase structures, *Heliobacter pylori* catalase (HPC; PDB code 1QWL), NADPH could not be definitely located.[51] It has been speculated that in this case, NADPH is possibly more loosely bound or bound in a different conformation. Normally, NADPH is bound in a pocket at the surface of the enzyme at a distance of ∼19 Å from the heme iron of the subunit. This is schematically displayed in Figure 1a for one subunit of HEC. The channel through which hydrogen peroxide approaches the active site is also indicated (see refs 4 and 6 for stereo views). The distance between carbon atom C4 of the dihydronicotinamide group of NADPH (i.e., the position of the reducing hydride) and the 4-vinyl group of heme (carbons marked blue in Figure 1a) is ∼13 Å (dotted line in Figure 1a). The space-filling presentation (Figure 1b) reveals that two protein chains cross between NADPH and heme. Arrows indicate the amino acid residues and the water molecule located between heme and NADPH, which are presumed to be of crucial importance for the reaction of Cpd I with NADPH (see below). A view of the NADPH binding pocket with and without bound NADPH is shown in Figure S1 in the Supporting Information.

In all catalases, a distal histidine (HIS) residue in proximity to the iron center (e.g., HIS75 in Figure 1b) serves as a proton shuttle, transferring a proton to the Cpd I-bound hydrogen peroxide in the second stage of the catalatic cycle. In catalases, two orientations of the heme ring with respect to the position of this histidine are realized, in which the histidine is located above pyrrole ring III or IV of the heme; these orientations are called HIS III and HIS IV, respectively. HIS IV is realized in Clade 1 and 2 catalases, while HIS III is found in Clade 3 catalases. The difference between HIS III and HIS IV is equivalent to a rotation of the heme about an axis through the meso carbons α and γ, as shown in Figure 2 using the structures of HEC and the Clade 2 catalase from *Escherichia coli* (HPII, PDB code 1GGE). The net effect of this formal rotation is that the positions of the vinyl (blue in Figure 2) and methyl groups of the heme are interchanged in Clade 3 catalases compared with those in Clades 1 and 2. The methyl and vinyl groups, respectively, in the rings of the porphyrin system are attached to C1 and C2 in ring I and to C3 and C4 in ring II.[54] Thus, in

(42) The PDB currently lists 76 entries under the keyword "catalase", including 52 structures of monofunctional catalases and 24 structures of catalase-peroxidases. Two of the monofunctional catalases belong to Clade 1, 17 to Clade 2, and 33 to Clade 3. The full list includes complete enzymes, subunits, substrate complexes, and catalytic intermediates.
(43) Carpena, X.; Soriano, M.; Klotz, M. G.; Duckworth, H. W.; Donald, L. J.; Melik-Adamyan, W.; Fita, I.; Loewen, P. C. *Proteins: Struct., Funct., Genet.* **2003**, *50*, 423–436.
(44) Hara, I.; Ichise, N.; Kojima, K.; Kondo, H.; Ohgiya, S.; Matsuyama, H.; Yumoto, I. *Biochemistry* **2007**, *46*, 11–22.
(45) Melik-Adamyan, W. R.; Bravo, J.; Carpena, X.; Switala, J.; Mate, M. J.; Fita, I.; Loewen, P. C. *Proteins: Struct., Funct., Genet.* **2001**, *44*, 270–281.
(46) Diaz, A.; Horjales, E.; Rudino-Pinera, E.; Arreola, R.; Hansberg, W. *J. Mol. Biol.* **2004**, *342*, 971–985.
(47) Ko, T. P.; Day, J.; Malkin, A. J.; McPherson, A. *Acta Crystallogr.* **1999**, *D55*, 1383–1394.
(48) Murshudov, G. N.; Grebenko, A. I.; Brannigan, J. A.; Antson, A. A.; Barynin, V. V.; Dodson, G. G.; Dauter, Z.; Wilson, K. S.; Melik-Adamyan, W. R *Acta Crystallogr.* **2002**, *D58*, 1972–1982.
(49) Gouet, P.; Jouve, H.-M.; Dideberg, O. *J. Mol. Biol.* **1995**, *249*, 933–954.
(50) Mate, M. J.; Zamocky, M.; Nykyri, L. M.; Herzog, C.; Alzari, P. M.; Betzel, C.; Koller, F.; Fita, I. *J. Mol. Biol.* **1999**, *286*, 135–149.
(51) Loewen, P. C.; Carpena, X.; Rovira, C.; Ivancich, A.; Perez-Luque, R.; Haas, R.; Odenbreit, S.; Nicholls, P.; Fita, I. *Biochemistry* **2004**, *43*, 3089–3103.
(52) Hakansson, K. O.; Brugna, M.; Tasse, L. *Acta Crystallogr.* **2004**, *D60*, 1374–1380.
(53) Riise, E. K.; Lorentzen, M. S.; Helland, R.; Smalas, A. O.; Leiros, H. K. S.; Willassen, N. P. *Acta Crystallogr.* **2007**, *D63*, 135–148.

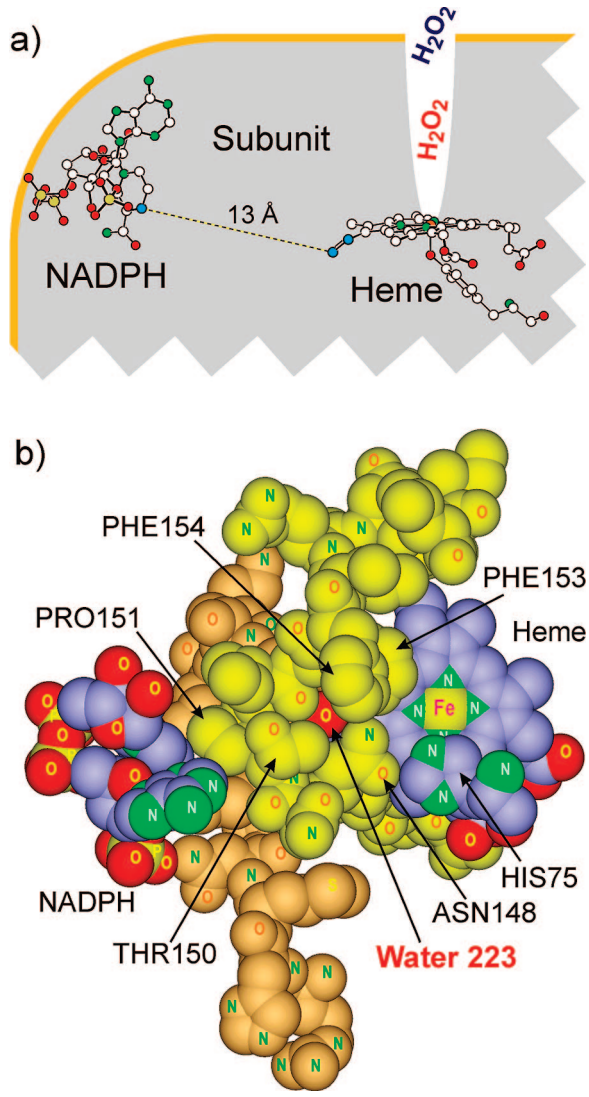

Figure 1. (a) Schematic and (b) space-filling representations of the heme−NADPH region of subunit A of HEC. In (b), the distal side of the heme is viewed.

Clade 3 catalases, the 4-vinyl group appears to be better positioned for electron transfer from NADPH.

Close inspection of the X-ray structures of Clade 3 catalases reveals a strikingly conserved amino acid sequence in the region between the heme and the NADPH binding site and an astonishingly similar arrangement of water molecules [Table 1 and Figure 3; details of the amino acid sequences (Table S1) and graphics showing the other structures (Figures S3−S5) are given in the Supporting Information]. In all but one of the cases, a serine residue that is part of a hydrogen-bonding network (see below) is found in close vicinity to the 4-vinyl group of heme (Figures 2 and 3). The only exception is the catalase from *Saccharomyces cerevisiae* (CatA). There, positions of the serine and the attached glycine residue in the amino acid sequence are interchanged (see Table S1). Remarkably, however, the local structural arrangement of the other Clade 3 catalases is essentially preserved in CatA because a water molecule (W19) adopts the position of the serine hydroxyl group (Table 1 and the top panel of Figure 3). The heavy-atom distances shown in

(54) For the numbering of the atoms of the catalase heme group, see: Fita, I.; Rossmann, M. G. *J. Mol. Biol.* **1985**, *185*, 21–37.

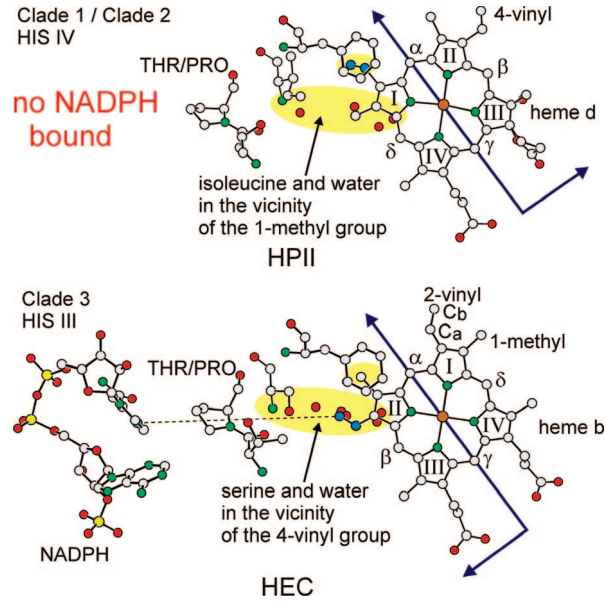

Figure 2. (top) HIS IV orientation in the Clade 2 catalase HPII. (bottom) HIS III orientation in the Clade 3 catalase HEC. Related space-filling representations are given in Figure S2 in the Supporting Information.

Figure 3 suggest the presence of substantial hydrogen bonding between these centers[55] (the computationally estimated hydrogen atom positions are displayed in Figure S4). Note that the relevant heavy-atom distances in HEC and CatA differ by 0.2 Å or less. Most importantly, in all of the NADPH-binding catalases except one, a water molecule that is almost symmetrically positioned between the heme 4-vinyl group and the THR−PRO couple (e.g., W223 in HEC and W671 in CatA) is part of a hydrogen-bonding network (see also Figures S3 and S4).[56] The O−C distances and the O−C−C angles demonstrate that this water is almost symmetrically placed between the two vinyl carbons and resides almost perpendicularly above the π system of the 4-vinyl group (with C4−C−C−O dihedral angles of 93 and 103° in HEC and CatA, respectively).

Figure 3 also displays the heme−NADPH region of HEC, including the conserved proximal tyrosine (TYR358) and arginine (ARG345) residues. A rather short distance of 3.8 Å between carbon C4 of the dihydronicotinamide group of NADPH and carbon C_G of PRO151 was found. Given the van der Waals radii of the hydrogen atoms attached to these atoms, such a distance clearly reflects a van der Waals contact between NADPH and PRO151.

In Clade 1 and 2 catalases, water molecules are not present in the direct neighborhood of the 2-vinyl group. In these enzymes, water molecules occupy spatial positions similar to those in Clade 3 catalases, placing them close to the 1-methyl group as a result of the rotated heme orientation (HIS IV). The 2-vinyl group is shielded by a conserved phenylalanine residue that in Clade 3 enzymes resides over the 3-methyl group (Figure

(55) Jeffrey, G. A.; Saeger, W. *Hydrogen Bonding in Biological Structures*; 2nd ed.; Springer: Berlin, 1994.

(56) The one exception for which no water at this position has been reported is BLC.[47] However, in the related crystal structure, fewer water molecules than in the other catalases have been detected. A feature similar to the chain of water molecules (W197, W21, W224, W171) on the proximal side of the heme of HEC shown in Figure 3 was also found in all of the other catalases except BLC (see Table S1 and Figure S5 in the Supporting Information). Thus, in BLC, the water may simply have escaped detection. Therefore, we suggest that this catalase should be reanalyzed.

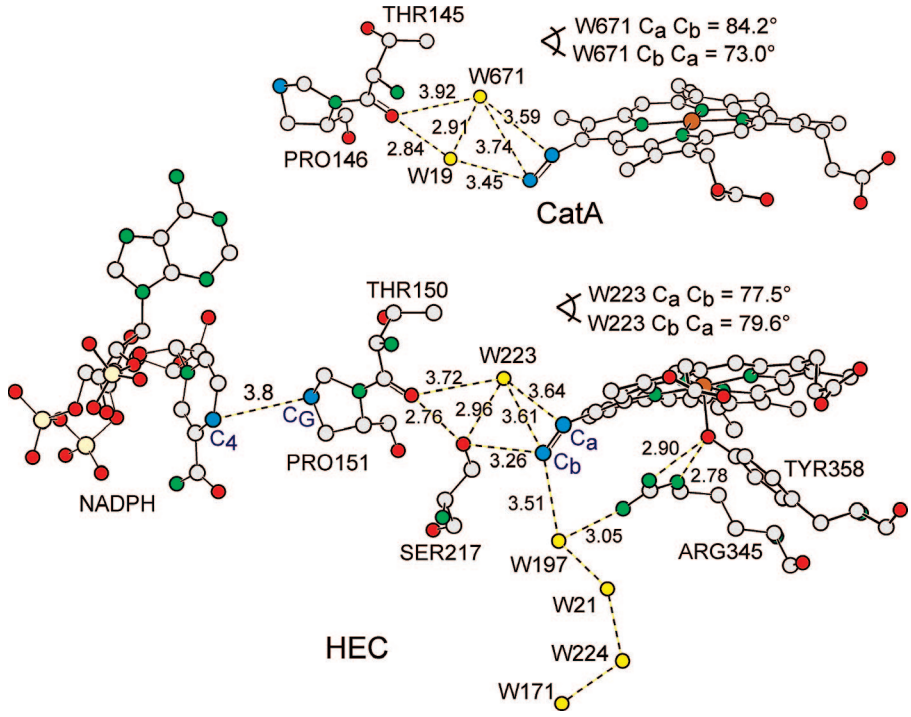

Figure 3. Relevant features in the X-ray structures of the Clade 3 catalases HEC and CatA in the vicinity of the heme 4-vinyl group. Atoms and residues are labeled according to PDB notation. Heavy-atom distances (dotted lines) are in angstroms. Key carbon and water oxygen atoms are highlighted blue and yellow, respectively. Similar representations of other Clade 3 catalases are shown in Figure S3 in the Supporting Information.

2). Furthermore, in Clade 1 and 2 enzymes, the hydrophobic amino acids valine and isoleucine, respectively, replace the serine of Clade 3 catalases (Table 1 and Table S1 in the Supporting Information).

Proposed Mechanism for the Prevention of Compound II Formation and Promotion of Electron Transfer. There seems to be a consensus that surface-bound NADPH acts as reducing agent to protect Cpd I of catalase against conversion to Cpd II. However, controversy exists about its action as a one- or two-electron donor. Consequently, various reducing mechanisms have been proposed.[11–17] One approach for solving the one- or two-electron problem is the postulate of electron tunneling from NADPH to the heme center. Accordingly, pathways for electron tunneling have been calculated.[12,14,15] On the other hand, because of the kinetic peculiarities of the action of NADPH, formation of a reducible intermediate, Cpd II′, has been proposed.[2,4,13,16] As mentioned in the Introduction, it is generally assumed that Cpd II is formed from Cpd I via Cpd I* by electron transfer from easily oxidizable amino acid residues, preferably tyrosine or tryptophan.[4,57] This would generate radical centers in the protein (porFe^{IV}=O/protein$^{\bullet}$), which indeed have been detected by EPR spectrometry in the absence of NADPH.[17,57,58] The opinion has been promoted that Cpd I first generates an amino acid radical by one-electron oxidation and that NADPH then donates one electron to re-reduce the amino acid radical and transfers the other electron to the heme iron, thus giving back ferricatalase.[13] However, there are several difficulties with such a mechanism.[4,16] For instance, it has been found that the EPR-detected tyrosyl radical is not located on the calculated pathway of electron tunneling from NADPH.[6,12,14,15] This is because radical centers may "travel" rapidly through the protein until a longer-lived, spectroscopically observable thermodynamic sink, e.g., a tyrosyl radical, is generated.[57] Further, since only one electron at a time would be transported via a protein radical intermediate, the other electron has to travel via a different route or the same protein radical has to be produced twice. Such a scenario, which would unfavorably affect the kinetics and efficiency of Cpd I reduction, intuitively appears to be rather unsatisfying for a general protection mechanism.

Analysis of the X-ray structures outlined above in essence revealed an identical structural motif in the NADPH−heme region of all Clade 3 catalases. Since this motif is not found in the non-NADPH binding Clade 1 and Clade 2 catalases, we believe that this highly conserved molecular arrangement is likely to have a functional role with regard to the physiological action of NADPH. In particular, the orientation of the 4-vinyl group of the heme toward the NADPH binding site and the presence of an adjacent water molecule are intriguing and seem to be of key importance. In the various classes of heme enzymes, the vinyl groups have been found or proposed to exert several functional roles. For example, the vinyl group is used for covalent linking of the heme with the protein under oxidative or reductive conditions,[59–63] serves as the target for protonation of heme[64] and a target for electrophile or radical addition,[65–67] and has been assigned an antenna function for conformational

(57) Svistunenko, D. A. *Biochim. Biophys. Acta* **2005**, *1707*, 127–155.
(58) Ivancich, A.; Jouve, H. M.; Gaillard, J. *J. Am. Chem. Soc.* **1996**, *118*, 12852–12853.
(59) Pipirou, Z.; Bottrill, A. R.; Metcalfe, C. M.; Mistry, S. C.; Badyal, S. K.; Rawlings, B. J.; Raven, E. L. *Biochemistry* **2007**, *46*, 2174–2180.
(60) Vu, B. C.; Jones, A. D.; Lecomte, J. T. J. *J. Am. Chem. Soc.* **2002**, *124*, 8544–8545.
(61) Rios-Velazquez, C.; Cox, R. L.; Donohue, T. J. *Arch. Biochem. Biophys.* **2001**, *389*, 234–244.
(62) Stevens, J. M.; Uchida, T.; Daltrop, O.; Ferguson, S. J. *Biochem. Soc. Trans.* **2005**, *33*, 792–795.
(63) Thöny-Meyer, L. *Biochemistry* **2003**, *42*, 13099–13105.
(64) Chiavarino, B.; Crestoni, M. E.; Fornarini, S.; Rovira, C. *Chem.—Eur. J.* **2007**, *13*, 776–785.

interaction with the protein[68,69] or electron transfer.[12,70] In fact, in calculations of the electron-tunneling pathway from NADPH to the heme center in bovine liver catalase (BLC), it has been assumed that electron transfer proceeds to the 4-vinyl group via the THR−PRO pair and the SER residue.[12,14,15] Therefore, and not surprisingly, modification of the vinyl group may alter the reactivity of the porphyrin system.[71] Accordingly, in 1960, Chance[72] reported on the reduced reactivity of Cpd II from horseradish peroxidase toward the donors ascorbic acid and uric acid upon vinyl modification, whereas the formation of Cpd I remained unaffected.

Considering the foregoing observations, we here present a new proposal for the mechanism of prevention of Cpd II formation and promotion of electron transfer from NADPH in Clade 3 catalases. At the center of our mechanism is a proposal for the structure of the elusive heme-derived intermediate Cpd II′, which is formed reversibly from Cpd I in competition with the second step of the catalatic cycle, the reduction of Cpd I by H_2O_2. In view of the high rate of the Cpd I + H_2O_2 reaction ($k = 3-4 \times 10^7$ M^{-1} s^{-1}),[9,18,73,74] formation and conversion of Cpd II′ becomes kinetically important only in situations where the lifetime of Cpd I is increased, i.e., when insufficient H_2O_2 is available to maintain the catalatic cycle. The formal steps of our mechanism are schematically displayed in Scheme 2.

When Cpd I (Scheme 2a) is formed in the first step of the catalatic cycle, nucleophilic attack on the double bond, i.e., an "umpolung" (polarity reversal) of the common electrophilic addition to C=C bonds, is facilitated: nucleophilic addition of OH^- released from the adjacent water can take place, with a simultaneous shift of the protons in this chain to create a positive charge on the proline residue that is in van der Waals contact with NADPH. Charge recombination by OH^- addition (which can be expected to be reversible) produces Cpd II′ ($HO-por^{\bullet}Fe^{IV}=O$), which bears a neutral, delocalized, carbon-centered π radical ($por^{\bullet}$) (Scheme 2b). The $por^{\bullet}$ radical is expected to be a much weaker oxidant than the related radical cation ($por^{\bullet+}$), and hence, the surrounding enzyme is protected against oxidative attack (one-electron transfer or hydrogen abstraction). As a result of the reduced reactivity, the lifetime of Cpd II′ should be greater than that of Cpd I, so reduction by NADPH should be kinetically enhanced. The positive charge on the THR−PRO residue is further proposed to increase the driving force for electron transfer from NADPH to heme and also to guide the electron flow along this chain of atoms. Two-electron transfer corresponds to reduction of the Fe^{IV} center and formal reduction of the porphyrin radical to the corresponding anion, as symbolized by the bracketed structure in Scheme 2. This reduction provides the driving force for spontaneous elimination of OH^- (as water) from the porphyrin system by

Scheme 2. Proposed Mechanism for NADPH-Mediated Conversion of Cpd I to Ferricatalase via Cpd II′

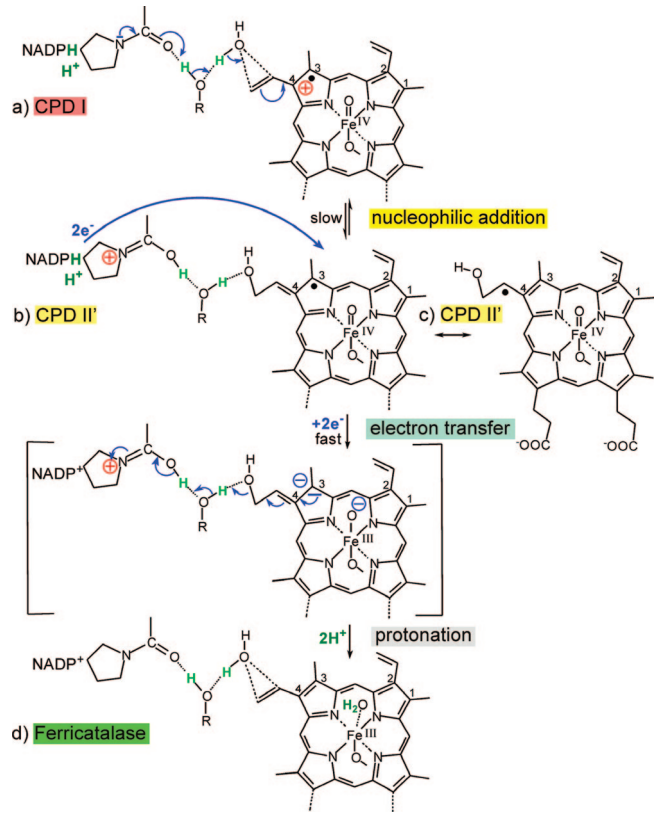

shifting of the protons back to the THR−PRO residue, and upon protonation, the system reverts to the enzyme's ferricatalase resting state (Scheme 2d). Notwithstanding, the order of the electron-transfer and protonation steps may be reversed.[75] The basic difference between our mechanism and previous mechanistic proposals is the decisive role of the water molecule that is involved in a reversible chemical transformation of the heme.

DFT Calculations on the Proposed Prevention of CPD II Formation and Promotion of Electron Transfer. The starting structure **A** used in the calculations was composed of a ferryloxoporphyrin group with a proximal phenolate ligand to which a methylguanidinium is hydrogen-bonded, two water molecules (W1 and W2), and an *N*-acetylpyrrolidine (NAP) group (Figure 4, top) and was obtained using the experimental coordinates of the related heavy atoms of HEC as well as their relative conformational arrangement (compare to Figure 3). The NAP group served as a model for the THR150−PRO151 couple of HEC and water W2 modeled SER217 of HEC. Except for the 4-vinyl group, the side chains of protoporphyrin IX were omitted. Several stable conformers of **A** were found, depending on the starting orientation of water molecules W1 and W2; however, these conformers differed only marginally (<1 kcal mol^{-1}) in energy. The lowest-energy optimized structure of **A** is shown in Figure 4. Superpositions of the HEC X-ray data and the computed structures of **A** (Figure S6 in the Supporting Information) demonstrate the preservation of the overall arrangement of the groups within the hydrogen-bonded complex.

(65) Wojciechowski, G.; Ortiz de Montellano, P. R. *J. Am. Chem. Soc.* **2007**, *129*, 1663–1672.
(66) Huang, L.; Wojciechowski, G.; Ortiz de Montellano, P. R. *J. Biol. Chem.* **2006**, *281*, 18983–18988.
(67) Huang, L. S.; Wojciechowski, G.; Ortiz de Montellano, P. R. *J. Am. Chem. Soc.* **2005**, *127*, 5345–5353.
(68) Boffi, A.; Zamparelli, C.; Verzili, D.; Ilari, A.; Chiancone, E. *Arch. Biochem. Biophys.* **1997**, *340*, 43–51.
(69) Smulevich, G.; Hu, S. Z.; Rodgers, K. R.; Goodin, D. B.; Smith, K. M.; Spiro, T. G. *Biospectroscopy* **1996**, *2*, 365–376.
(70) Gingrich, D. J.; Nocek, J. M.; Natan, M. J.; Hoffman, B. M. *J. Am. Chem. Soc.* **1987**, *109*, 7533–7534.
(71) Zhu, Y.; Silverman, R. B. *J. Org. Chem.* **2007**, *72*, 233–239.
(72) Chance, B.; Paul, K. G. *Acta Chem. Scand.* **1960**, *14*, 1711–1716.
(73) Chance, B. *J. Biol. Chem.* **1949**, *180*, 947–959.
(74) Jakopitsch, C.; Vlasits, J.; Wiseman, B.; Loewen, P. C.; Obinger, C. *Biochemistry* **2007**, *46*, 1183–1193.

(75) It should be noted that in earlier calculations of possible electron-tunneling pathways,[12,14,15] the THR−PRO couple adjacent to NADPH (THR149−PRO150 in BLC) in fact was located as the first relay, from which one of two favorable electron paths to the heme vinyl involves the serine residue (e.g., SER216 in BLC).

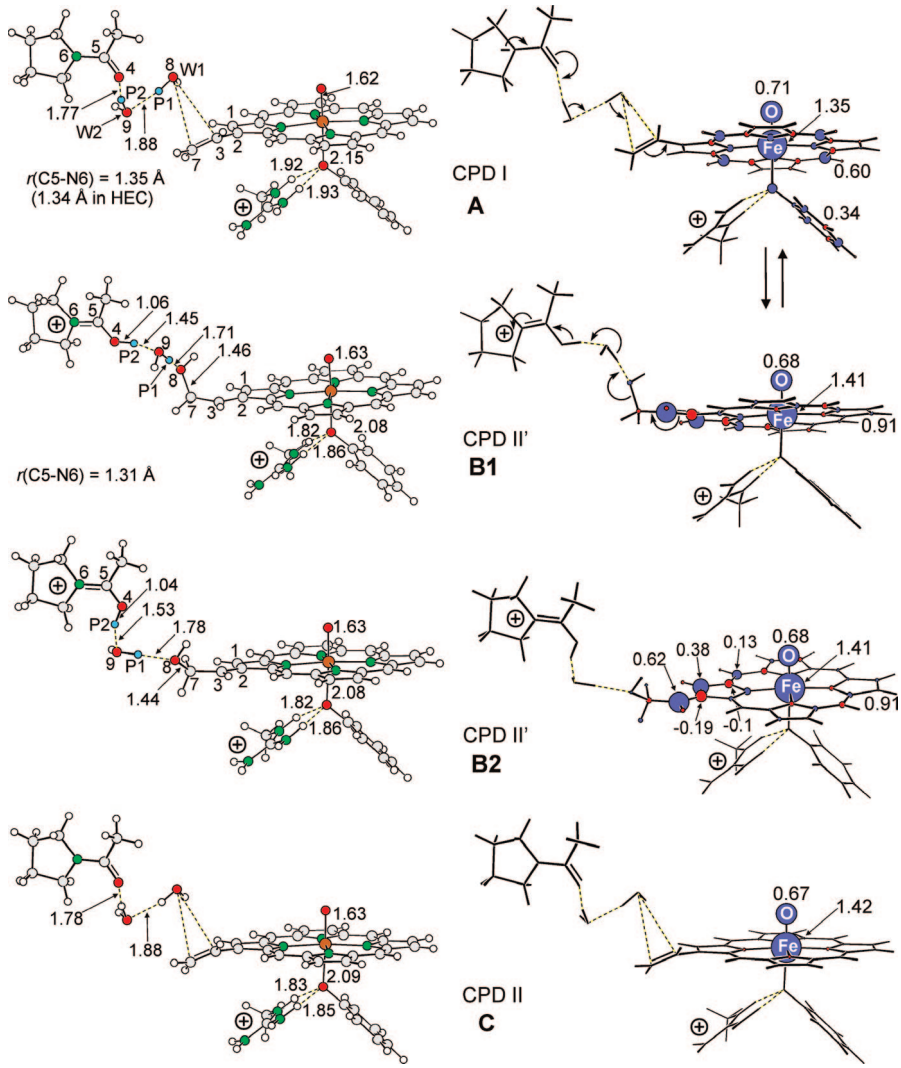

Figure 4. (left) Optimized (SCRF−B3LYP/6-31G*) structures and (right) related unpaired spin densities of structural models: **A**, representing the initial arrangement of the key molecules for reduction of Cpd I by NADPH; **B1** and **B2**, representing two conformers of Cpd II′, the product of nucleophilic addition of OH^- to the vinyl group of the heme center; and **C**, representing Cpd II, the product of one-electron reduction of Cpd I. The hydrogens that are translocated within the hydrogen-bonded network are colored blue in the structures on the left. Bond lengths are in angstroms. On the right, positive and negative spin densities are indicated by blue and red circles, respectively, and refer to the high-spin states; the size of each circle corresponds to the fraction of unpaired spin density at that center. The low-spin structures of **A** and **B1** are shown in Figure S9 in the Supporting Information.

In particular, W2 indeed remained close to the position of the hydroxyl group of SER217.

Two stable OH^- adducts, labeled **B1** and **B2** in Figure 4, were found; the experimental atomic arrangement of HEC was somewhat better conserved in **B2** than in **B1** (Figure S7 in the Supporting Information). In accord with our proposed mechanism, both optimized structures confirm that when water W1 attacks the vinyl group, a proton is released and migrates to the oxygen atom of W2 while a proton of W2 is simultaneously shifted to the carbonyl oxygen O4 of NAP. Figure 4 also reveals that the hydrogen-bonding network of **A** is retained in **B1** and **B2**. As clearly indicated by the computed dipole moments (Table 2) and atomic charges (Figure S8 in the Supporting Information), the positive charge of the porphyrin radical cation of Cpd I was relocated to the THR−PRO residue, as depicted in Scheme 2b.

The calculated spin densities (ρ) given in Figure 4 show that in its high-spin quartet state ($S = {}^3/_2$), the Cpd I model **A** is characterized by two unpaired electrons residing on the Fe^{IV}═O group ($\rho_{total} = 2.06$) and one unpaired electron delocalized over the porphyrin π system ($\rho_{total} = 0.60$) and the proximal phenolate ligand ($\rho = 0.34$), in agreement with previous calculations.[31,33,76,77] Addition of OH^- leads to charge recombination, but the distribution of the unpaired spin density in the Cpd II′ models **B1** and **B2** is essentially unchanged, with two electrons located on Fe^{IV}═O ($\rho_{total} = 2.09$) and one unpaired electron residing on the porphyrin ring ($\rho_{total} = 0.91$). It should be noted that the spin density of this neutral porphyrin π radical is mainly (~80%) located on carbon atoms C3 of the vinyl group and C1 and C2 of pyrrole ring II, thus rendering this radical essentially an allyl-type species, as visualized in the resonance structures shown in Scheme 2b,c. It is also noteworthy that in structures **B1** and **B2**, no unpaired spin density is transferred to the proximal phenolate ligand, whereas in **A**, 34% of the unpaired spin is found on this group.

Apart from the radical nature of the porphyrin ring, Cpd II′ is predicted to be very similar to Cpd II. This is evident from comparison of **B1** and **B2** with the related Cpd II model **C**, for

(76) de Visser, S. P. *Inorg. Chem.* **2006**, *45*, 9551–9557.
(77) Barea, G.; Maseras, F.; Lledos, A. *THEOCHEM* **2003**, *632*, 323–333.

which a virtually identical spin density distribution on the Fe^{IV}=O group and almost no unpaired spin on the proximal phenolate were found. Thus, the open-shell nature of the porphyrin in **B1** and **B2** does not noticeably affect the electronic properties of the ferryloxo center. This is also reflected by the lengths of the Fe−phenolate bonds in **B1** and **C** (2.08 and 2.09 Å, respectively), both of which are shorter than the one in **A** (2.15 Å). The strong similarity of Cpd II and Cpd II′ is also evident from the changes in the atomic charge distribution of the heme group when these species are formed from Cpd I, which demonstrate that both are one-electron reduction products of Cpd I in which the electron has been transferred to the porphyrin π system (Figure S8 in the Supporting Information).[78]

Since reduction of Cpd I by NADPH kinetically competes with the second step of the catalatic cycle (Cpd I + H_2O_2) as well as with deactivation to Cpd II by electron transfer from the protein, the feasibility of the mechanism proposed here strongly depends on the energetics of the **A** → **B** transformation. The electronic energies of **B1** relative to **A** at 0 K (E_{rel}) were calculated to be −4.4 and −5.3 kcal mol^{-1} for ε = 5.7 and 10.65, respectively, whereas **B2** was found to be lower in energy than **A** by 0.3 or 1.6 kcal mol^{-1} (Table 2). Inclusion of the ΔZPVE estimate (+4.6 kcal mol^{-1}) places these E_{rel} values at approximately +0.2 and −0.7 kcal mol^{-1} for **B1** and +4.3 and +3.0 kcal mol^{-1} for **B2**. Of course, in view of the simplifications which had to be made in the calculations, these energy changes should only be considered as rough estimates. Nevertheless, it seems legitimate to assume that the free-energy levels of **A** and of **B1** and **B2** are close enough to allow the formation of a rapid equilibrium between these structures,[79] provided that the activation barrier for the **A** ⇌ **B** transformation is sufficiently low (see below).

To estimate the activation barrier of the proposed Cpd I ⇌ Cpd II′ transformation and the energetics of regenerating the ferricatalase resting state from Cpd II′, a model even more simplified than **A** ⇌ **B1/B2** was designed. In this model, the high complexity of the hypersurface of a system incorporating two more-or-less concerted proton shifts was reduced to a simple reaction coordinate, namely, variation of the HO−vinyl distance. The basic features of the model are the coplanarity of the 4-vinyl group with the porphyrin ring and the omission of one water molecule (W2), as shown in Figure 5 (this figure uses different numbering of atoms than Figure 4; further details are given on p S12 in the Supporting Information). Optimizations of **1** and the OH^- adduct **2** with the C1−C2−C3−O4 dihedral angle fixed at 90° gave electronic energies of **2** that were just −0.3 and −1.4 kcal mol^{-1} lower than those of **1** for ε = 5.7 and 10.65, respectively (Table 2). Upon inclusion of the ΔZPVE correction (+4.6 kcal mol^{-1}), Cpd II′ model **2** is predicted to be 3−4 kcal mol^{-1} less stable than **1**, i.e., an energy difference similar to that calculated for the **A** ⇌ **B1/B2** system is observed. Likewise, the structural and electronic characteristics are quite similar. Thus, use of the simplified models **1** and **2** appears to be justified.

The maximum-energy structure TS[RC] **3**, which should be a reasonably good approximation of the true TS, was found at an O4−C3 distance of 1.9 Å. The energy of **3** is 8.2 (ε = 5.7) or 7.8 (ε = 10.65) kcal mol^{-1} higher than that of the starting complex **1**. The elongation of the O−H bond of W1 directed toward O5 (1.03 Å) and the shortening of the hydrogen bond from 1.87 Å in **1** to 1.57 Å in **3** clearly indicate the movement of the proton from W1 to the carbonyl group of NAP. The charge-separation process is also indicated by an increase of the dipole moment to 27.0 D. By roughly estimating the change in ZPVE in going from **1** to **3** to be 2.0 kcal mol^{-1} [about half of the difference (4.6 kcal mol^{-1}) between the ZPVEs of **1** and **2**], we arrive at an energy barrier of 10 kcal mol^{-1} for the nucleophilic addition of OH^- to the vinyl group of heme. Thus, a sufficiently fast equilibrium between Cpd I and Cpd II′ at physiological temperatures can be assumed.

The question of whether Cpd II′ would be a favorable intermediate for reversion back to ferricatalase remains. Our model demands that transfer of two electrons from NADPH to Cpd II′ and additional protonation enforces the elimination of water to regenerate the 4-vinyl group at heme. To accommodate this, one electron must be transferred to the ferryloxo group while the other is used to reduce the neutral porphyrin radical (represented by the bracketed structure in Scheme 2). A true hydride transfer across such a distance seems to be highly unlikely and is excluded. We therefore performed calculations on several structures in which the required electrons and protons were added to models **1** and **2**, utilizing 1-methyl-1,4-dihydropyridine-3-carboxylic acid amide [*N*-methyldihydronicotinamide (NMNAH)] as a model for the formal hydride (i.e., $H^+ + 2e^-$) donor NADPH. In order to preserve the overall charge balance, the additional protonation step was calculated using imidazolium as the proton source, thereby modeling the action of the distal histidine residue of native catalase. In the final ferricatalase model **4**, the produced water molecule was left coordinated to the Fe^{III} center. The energy data in Figure 5 are energies relative to Cpd I model **1** + imidazolium + NMNAH (Table 2). It should be emphasized that we do not intend the computed structures connecting **1** and **2** with **4** to be considered as true intermediates in this process; rather, they should be regarded as rationalizations for the chemical transformations and estimates of the energy changes which must take place in order to restore the resting state of the enzyme.

The overall process **2** (Cpd II′) → **4** (ferricatalase) is highly exoergic ($\Delta E \approx -57$ kcal mol^{-1}). If **2** is formally reduced by a hydride ion to give the Fe^{III} hydroxide complex **5** (path **a** in Figure 5), 45 kcal mol^{-1} of the total driving force is provided by this step and the additional 12 kcal mol^{-1} is produced by subsequent protonation of the distal hydroxyl ligand. Interestingly, protonation of **2** prior to NADPH reduction also appears to be feasible (path **b** in Figure 5), because the energy of the protonated complex **6** is predicted to be almost identical to that of **2** [E(**6**) − E(**2**) = −0.2 kcal mol^{-1}]. In this case, the entire driving force for formation of **4** is now derived from the addition of $H^+ + 2e^-$. It is worth noticing that the spin density distribution in **2** is not much affected upon protonation of the ferryloxo group, apart from some redistribution within this group: iron in complex **6** remains in the high-spin Fe^{IV} state, and the neutral π radical nature of the porphyrin ring is preserved. On the way from **2** or **6** to **5** or **4**, respectively, no

(78) There is in fact an ambiguity with respect to the use of the notation Cpd II′ (as opposed to Cpd I′) for our proposed intermediate HO−por$^{\bullet}$$Fe^{IV}$=O. In terms of unpaired electrons (of which it has three, i.e., two electrons missing from the resting state), it is in fact closer to Cpd I, but in terms of geometry and spin density at the Fe=O center, it much more resembles Cpd II (as shown by a comparison of the data in Figure 4 and Figure S8 in the Supporting Information). It should be noted that a similar ambiguity exists in designating porFe^{IV}=O/protein$^{\bullet}$, the product of one-electron reduction of Cpd I by the surrounding protein, as Cpd I* (see the Introduction).

(79) If the reasonable assumption that $\Delta G \approx \Delta E$ is made, these data correspond to values ranging from 7×10^{-4} to 3.3 for the equilibrium constant K_{eq}.

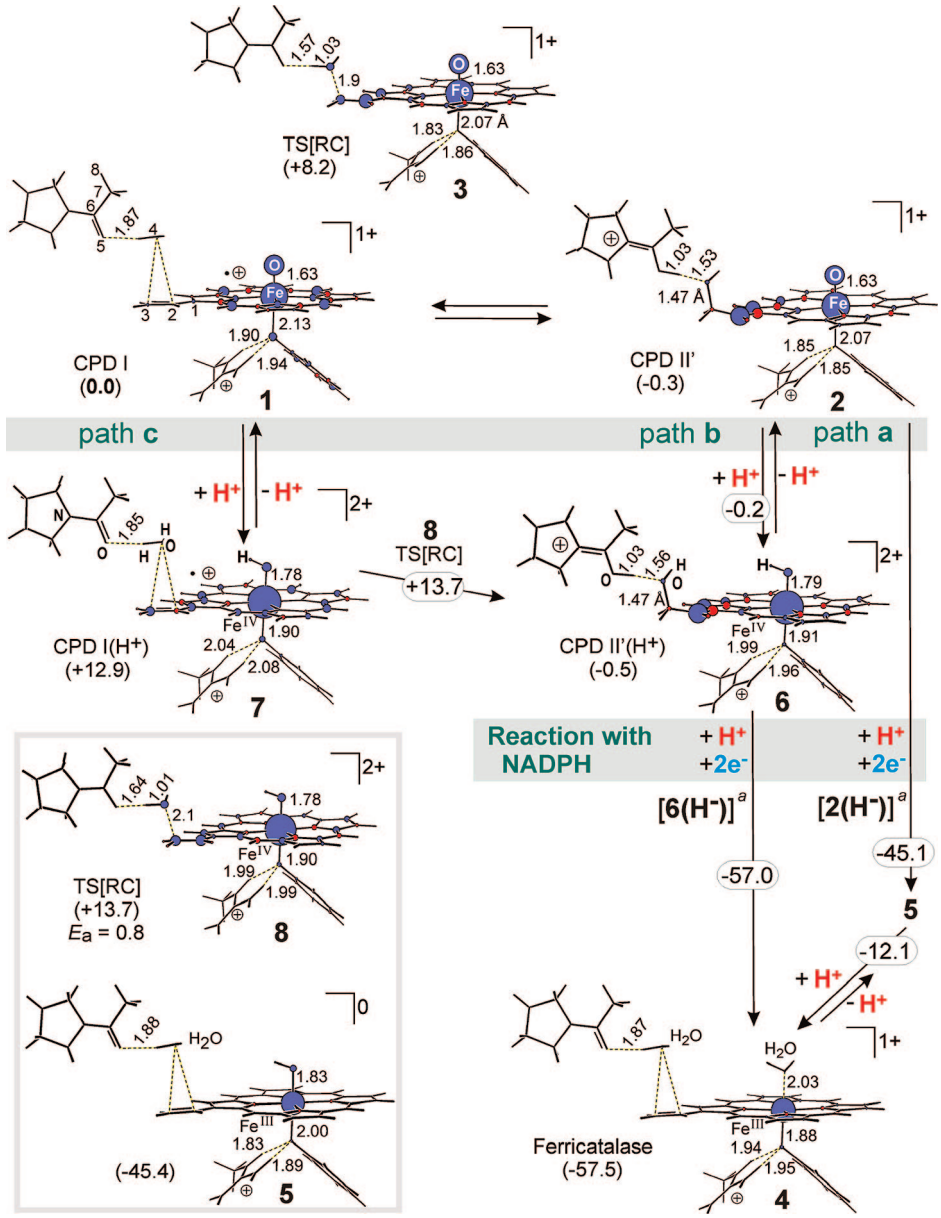

Figure 5. Structures, spin densities, and energies (kcal mol^{-1}) for conversion of Cpd I model **1** to the high-spin Cpd II′ model **2** and regeneration of the low-spin ferricatalase model **4**. *a*Structures of **6**(**H**$^-$) and **2**(**H**$^-$) are shown in Figure S10 in the Supporting Information.

stable intermediate could be located. Upon optimization, addition of $H^+ + 2e-$ to **2** or **6** resulted in barrierless elimination of OH^- to directly give **5** or **4**, respectively.[80] The large exothermicity and the fact that protonation does not seem to affect the reducibility of **2** provide conclusive evidence that Cpd II′ is a favorable intermediate for rapid conversion of Cpd I to ferricatalase.

The finding that Cpd I model **1** and Cpd II′ models **2** and **6** are energetically almost degenerate suggested that formation of Cpd II′ and subsequent regeneration of ferricatalase might also proceed via initial protonation of Cpd I (path **c** in Figure 5). This turned out to be possible, but as demonstrated by structure **7**, protonation of Cpd I is endoergic by 11−13 kcal mol^{-1}, which can reasonably be explained by charge repulsion from the cationic porphyrin system. On the other hand, the increased overall charge of the heme system of **7** would further facilitate nucleophilic addition of OH^- from water W1 to give protonated Cpd II′ (**6**). This addition is driven by an energy release of ∼13 kcal mol^{-1} and should proceed essentially without a barrier, as the approximate transition structure **8** was computed to be only ∼1 kcal mol^{-1} above **7**. The foregoing data conclusively suggest that the regeneration of ferricatalase (**4**) should be fast irrespective of the initial protonation state of Cpd I and/or Cpd II′, with formation of the protonated Cpd II′ model **6** via **3** and **2** to be kinetically favored by ∼4 kcal mol^{-1} over the pathway via **7** and **8**.

A key feature of NADPH-mediated conversion of Cpd I to ferricatalase is the fact that NADPH acts as a two-electron donor.

(80) When the C3−O4H bonds in **2** and **6** were fixed at 1.47 Å in the optimizations, the corresponding hypothetical reduced intermediates **2**(**H**−) and **6**(**H**−) (see Figure S10 in the Supporting Information) were computed to be stabilized by 4.1 and 24.7 kcal mol^{-1} with respect to **2** and **6**, respectively, i.e., their energies were 41.3 and 32.8 kcal mol^{-1} greater than those of products **5** and **4**. Since structures **2**(**H**−) and **6**(**H**−) in turn would represent the initial products of nucleophilic OH−addition to complex **5** and ferricatalase **4**, respectively, it is evident that such an addition is highly unlikely to occur.

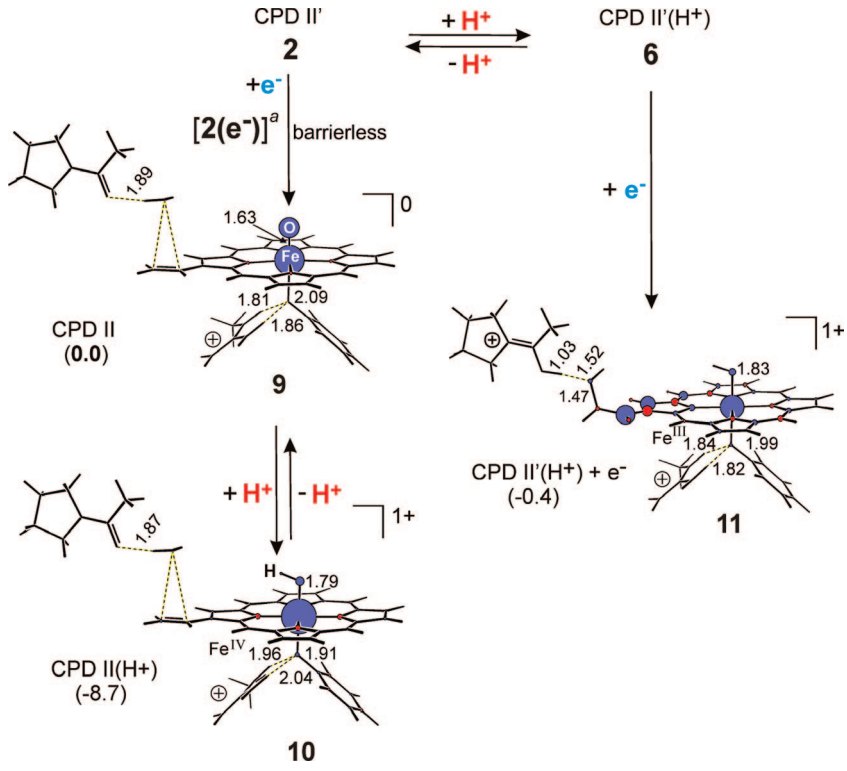

Figure 6. Structures, spin densities, and energies (kcal mol^{-1}) of one-electron reduction products from Cpd II′. [a]The structure of **2**(**e**$^-$) is shown in Figure S10 in the Supporting Information.

As mentioned above, in the presence of typical one-electron donors such as ascorbic acid or phenols, Cpd I is rapidly converted to Cpd II.[2–7,9] Most interestingly, it has recently been observed that decay of Cpd I from BLC in the presence of ascorbate (which gives Cpd II) follows virtually the same kinetics as that in the presence of NADPH (which yields ferricatalase).[81] This unexpected observation not only suggests that ascorbate might bind at the same site as NADPH but also implies the same rate-limiting step for both reductions. This step would likely be OH^- addition to the 4-vinyl group of Cpd I, as proposed here. We therefore performed calculations on a few additional structures in order to check whether Cpd II′ might also be a viable intermediate for Cpd II formation by external one-electron reductants. The results are displayed in Figure 6 and Table 2 (energies are given relative to Cpd II model **9**). When an electron was added to structure **2**, barrierless release of OH^-/H_2O to give **9** directly was observed upon optimization.[82] Thus, one-electron reduction of Cpd II′ efficiently reverses nucleophilic OH^- addition to Cpd I. This clearly demonstrates that a positive charge on the porphyrin system, which is present only in Cpd I, is indispensable for nucleophilic addition of OH^-. Furthermore, formation of Cpd II via one-electron reduction of Cpd II′ interrupts the favorable pathway for subsequent electron transport. This consequence nicely corresponds with the experimental observation that NADPH is quite ineffective in converting Cpd II back into ferricatalase.[2–4,6] On the other hand, the facile conversion of Cpd II′ to Cpd II (**2** → **9**) by one-electron reduction would then suggest that in the regeneration of ferricatalase from Cpd II′, the two electrons must be transferred from NADPH essentially simultaneously in order to avoid blocking of the second electron transfer by Cpd II formation via transfer of the first electron. The general assumption that Cpd II may preferably exist in a protonated form (porFe^{IV}−OH$^+$)[2,83] has recently been theoretically and experimentally confirmed.[22–24] This is also supported by our data, which show that the protonated Cpd II model **10** is stabilized by 8.7 or 5.4 kcal mol^{-1} for $\varepsilon = 5.7$ or 10.65, respectively. It is noteworthy that in contrast to what was observed for **2**, one-electron reduction of protonated Cpd II′ (**6**) gave a stable product (**11**) having an energy similar to that of Cpd II ($E_{rel} = -0.4/+1.5$ kcal mol^{-1} for $\varepsilon = 5.7$ or 10.65, respectively). Calculations on **11** showed that the Fe^{IV} center was reduced to Fe^{III} but the OH^- substitution of the porphyrin radical was preserved. Thus, structure **11** is still a viable structure for electron transport via the proposed pathway.

Conclusion

The mechanism by which surface-bound NADPH in monofunctional Clade 3 catalases protects the reactive intermediate Cpd I against deactivation by one-electron reduction to catalytically inactive Cpd II has been subject of intense research for more than 20 years. The accumulated experimental evidence has led to the hypothesis that NADPH rapidly converts Cpd I back to the enzyme's resting state (ferricatalase) via two-electron reduction of an intermediate named Cpd II′, which should be

(81) Kirsch, M.; Auferkamp, O.; Meier, A.-C.; Korth, H.-G.; Sustmann, R.; de Groot, H. Universität Duisburg-Essen. Unpublished results, 2007.

(82) With the C3−O4H bond fixed at 1.47 Å, the energy of **2**(**e**$^-$), the one-electron reduction product of **2**, was estimated to be 40 kcal mol^{-1} higher than that of **9** (see Figure S10 in the Supporting Information). The system utilized the extra electron for reduction of the porphyrin radical to the corresponding anion rather than for reduction of the Fe^{IV} center.

(83) Berglund, G. I.; Carlsson, G. H.; Smith, A. T.; Szoke, H.; Henriksen, A.; Hajdu, J. *Nature* **2002**, *417*, 463–468.

in equilibrium with Cpd I. To date, no satisfying mechanism for this process has been provided.

In the present study, analysis of the available X-ray structures of various catalases revealed that the NADPH-binding Clade 3 catalases exhibit a strikingly conserved molecular arrangement in the region of the subunit between the heme and the NADPH binding site. A unique feature of this substructure is the presence of a water molecule adjacent to the 4-vinyl group of the heme. We have proposed a mechanism in which this water molecule plays a pivotal role in the conversion of Cpd I to ferricatalase. The crucial step of the proposed mechanism is nucleophilic addition to the terminal carbon atom of the 4-vinyl group by a hydroxide ion released from the water molecule; this process is driven by the positive charge on the porphyrin ring of Cpd I. The HO−porphyrin adduct thus formed includes a ferryloxo (Fe^{IV}═O) center and a neutral π radical of the porphyrin (por$^{\bullet}$) and is believed to be the elusive Cpd II′ intermediate proposed earlier.

The proposed mechanism is supported by the results of DFT calculations on appropriate model structures. The computed structures and energies of the mechanistic steps are in full accord with the following requirements for the intermediate Cpd II′ as summarized in recent reviews:[2,4] (1) a rate of formation that is small compared with that of the reaction of Cpd I with H_2O_2 but significantly larger than that for reduction of Cpd I to Cpd II by one-electron transfer from the surrounding protein or other exogenous donors; (2) existence of an equilibrium between it and Cpd I; (3) rapid reduction by two-electron transfer from NADPH, thereby leading to (4) direct reconversion to ferricatalase; and (5) a structure similar to Cpd II. Furthermore, the proposed OH^- adduct to Cpd I is also predicted to be a viable intermediate for the reduction of Cpd I to Cpd II by exogenous one-electron donors such as ascorbate in the absence of NADPH. Particularly attractive features of the proposed mechanism are that formation of a functional protein radical is not required and that the process is independent of the protonation states of intermediates Cpd I and Cpd II′. To summarize, our mechanistic model takes into account the structural, kinetic, and electronic characteristics of the catalase enzymes and satisfies the requirements summarized recently by Kirkman and Gaetani.[4] Efforts to find experimental (spectroscopic) evidence for the nature of Cpd II′ as proposed here are in progress.

We also note here that the current analyses of the X-ray structures of three catalase-peroxidases and ten peroxidases have disclosed an amazingly similar placement of water molecules in the vicinity of the 2-vinyl group of heme.[84] Therefore, in these enzymes, reversible nucleophilic addition of OH^- to Cpd I may also occur. Since no NADPH is available in these enzymes to convert the Cpd II′ species thus formed back to the resting state, formation of Cpd II′ would now serve to protect Cpd I against unwanted side reactions in order to ensure electron flow from the substrate binding site at the surface region of the protein. In conclusion, the presence of a functional water molecule next to the vinyl group of the heme is hypothesized to be a general phenomenon in the reaction of a variety of heme enzymes. *There is no fundamental difference between the peroxidase and catalase reactions; catalase activity appears to be the special case of peroxidase activity when the substrate and acceptor are identical.*[19]

Acknowledgment. This work was supported by the Deutsche Forschungsgemeinschaft (SFB 452). We thank the Hochschulrechenzentrum Duisburg-Essen for the generous allotment of computer resources.

Supporting Information Available: A table of partial amino acid and water sequences of 13 catalases, five figures showing partial structures of Clade 3 catalases, six tables of absolute and relative energy data, a table of distance and spin-density parameters, two tables and associated descriptions of computational constraints, seven figures showing computed structures and spin densities, complete ref 30, and Cartesian coordinates for all of the computed structures. This material is available free of charge via the Internet at http://pubs.acs.org.

JA077787E

(84) Sicking, W.; Korth, H.-G.; de Groot, H.; Sustmann, R. Universität Duisburg-Essen. Unpublished results.